

Effect of TbF_3 diffusion on the demagnetization behavior and domain evolution of sintered Nd-Fe-B magnets by electrophoretic deposition

Xue-Jing Cao(曹学静), Shuai Guo(郭帅), Yu-Heng Xie(谢宇恒), Lei Jin(金磊), Guang-Fei Ding(丁广飞), Bo Zheng(郑波), Ren-Jie Chen(陈仁杰), and A-Ru Yan(闫阿儒)

Citation: Chin. Phys. B, 2023, 32 (**9**): 097503. DOI: 10.1088/1674-1056/acaf2d
Journal homepage: http://cpb.iphy.ac.cn; http://iopscience.iop.org/cpb

What follows is a list of articles you may be interested in

Coercivity enhancement of sintered Nd-Fe-B magnets by grain boundary diffusion with $Pr_{80-x}Al_xCu_{20}$ alloys

Zhe-Huan Jin(金哲欢), Lei Jin(金磊), Guang-Fei Ding(丁广飞), Shuai Guo(郭帅), Bo Zheng(郑波),Si-Ning Fan(樊思宁), Zhi-Xiang Wang(王志翔), Xiao-Dong Fan(范晓东), Jin-Hao Zhu(朱金豪),Ren-Jie Chen(陈仁杰), A-Ru Yan(闫阿儒), Jing Pan(潘晶), and Xin-Cai Liu(刘新才)

Chin. Phys. B, 2023, 32 (**1**): 017505. DOI: 10.1088/1674-1056/ac6741

Coercivity and microstructure of sintered Nd-Fe-B magnets diffused with Pr-Co, Pr-Al, and Pr-Co-Al alloys

Lei Jin(金磊), Zhe-Huan Jin(金哲欢), Jin-Hao Zhu(朱金豪), Guang-Fei Ding(丁广飞), Bo Zheng(郑波) , Shuai Guo(郭帅), Ren-Jie Chen(陈仁杰), A-Ru Yan(闫阿儒), and Xin-Cai Liu(刘新才)

Chin. Phys. B, 2021, 30 (**2**): 027503. DOI: 10.1088/1674-1056/abc166

Improvement in coercivity,thermal stability,and corrosion resistance of sintered Nd-Fe-B magnets with $Dy_{80}Ga_{20}$ intergranular addition

Beibei Zhou(周贝贝), Xiangbin Li(李向斌), Xuejing Cao(曹学静), Gaolin Yan(严高林), Aru Yan(闫阿儒)

Chin. Phys. B, 2016, 25 (**11**): 117504. DOI: 10.1088/1674-1056/25/11/117504

Effects of terbium sulfide addition on magnetic properties, microstructure and thermal stability of sintered Nd—Fe—B magnets

Xiang-Bin Li(李向斌), Shuo Liu(刘硕), Xue-Jing Cao(曹学静), Bei-Bei Zhou(周贝贝), Ling Chen(陈岭), A-Ru Yan(闫阿儒), Gao-Lin Yan(严高林)

Chin. Phys. B, 2016, 25 (**7**): 077502. DOI: 10.1088/1674-1056/25/7/077502

Effect of TbF_3 diffusion on the demagnetization behavior and domain evolution of sintered Nd–Fe–B magnets by electrophoretic deposition

Xue-Jing Cao(曹学静)[1,2,†], Shuai Guo(郭帅)[1,2], Yu-Heng Xie(谢宇恒)[1,2], Lei Jin(金磊)[1,2], Guang-Fei Ding(丁广飞)[1,2], Bo Zheng(郑波)[1,2], Ren-Jie Chen(陈仁杰)[1,2], and A-Ru Yan(闫阿儒)[1,2]

[1] *CISRI and NIMTE Joint Innovation Center for Rare Earth Permanent Magnets, Ningbo Institute of Material Technology and Engineering, Chinese Academy of Sciences, Ningbo* 315201, *China*

[2] *CAS Key Laboratory of Magnetic Materials and Devices, Ningbo Institute of Material Technology and Engineering, Chinese Academy of Sciences, Ningbo* 315201, *China*

(Received 14 November 2022; revised manuscript received 22 December 2022; accepted manuscript online 30 December 2022)

We studied the magnetic properties and domain evolution of annealed and TbF_3-diffused sintered Nd–Fe–B magnets using the electrophoretic deposition method. After TbF_3 diffusion, the coercivity increased significantly by 9.9 kOe and microstructural analysis suggested that Tb favored the formation of the $(Nd, Tb)_2Fe_{14}B$ shell phase in the outer region of the matrix grains. The first magnetization reversal and the dynamic successive domain propagation process were detected with a magneto-optical Kerr microscope. For the TbF_3-diffused magnet, the magnetization reversal appeared at a larger applied field and the degree of simultaneous magnetization reversal decreased compared with an annealed magnet. During demagnetization after full magnetization, the occurrence of domain wall motion (DWM) in the reproduced multi-domain regions was observed by the step method. The maximum polarization change resulting from the reproduced DWM was inversely related to the coercivity. The increased coercivity for the diffused magnet was mainly attributed to the more difficult nucleation of the magnetic reversed region owing to the improved magneto-crystalline anisotropy field as a result of Tb diffusion.

Keywords: sintered Nd–Fe–B magnet, electrophoretic deposition, grain boundary diffusion, domain evolution

PACS: 75.50.Ww, 75.50.Vv, 75.60.–d, 75.60.Jk **DOI:** 10.1088/1674-1056/acaf2d

1. Introduction

Popularizing energy-saving rare earth permanent magnet motors and developing renewable wind power generation are effective ways to realize green and sustainable development. Nd–Fe–B permanent magnets are extensively applied in traction motors and wind power turbines owing to their excellent intrinsic magnetic properties, such as a high magneto-crystalline anisotropy field and maximum magnetic energy product.[1,2] The addition of heavy rare earth (HRE) elements (Dy and Tb) is a useful method to achieve high coercivity, which can meet the requirements of high-temperature applications.[3,4]

The nucleation mechanism of reverse domains was thought to be the predominant mechanism of magnetization reversal for sintered Nd–Fe–B magnets. The nucleation sites are usually the grain boundaries and the surface of $Nd_2Fe_{14}B$ grains, regions where the localized magneto-crystalline anisotropy field (H_A) is much lower.[5,6] Therefore, it is expected that substitution of HRE elements mainly occurs at grain boundaries and the outer region of $Nd_2Fe_{14}B$ grains. The grain boundary diffusion method has been widely reported: HRE elements diffuse from the surface to the interior of magnets primarily through grain boundaries, and then substitute for Nd in the outer region of matrix grains in this process.[7–9] Therefore, HRE elements introduced by grain boundary diffusion treatment can effectively harden the lower-H_A regions and substantially reduce the content of HRE elements in the preparation of high-coercivity magnets, but with a slight decrease in the remanence.[10–15]

It is well known that the coercivity of Nd–Fe–B permanent magnets is a parameter that is sensitive to microstructure. The relationship between the microstructure and the coercivity of sintered Nd–Fe–B magnets has been experimentally clarified. According to Refs. [16,17], both the higher H_A of a HRE-rich core–shell structure and the continuous Nd-rich grain boundary phase are conducive to improved coercivity. Furthermore, micromagnetic simulation indicated that the coercivity of grain boundary diffusion-processed sintered Nd–Fe–B magnets was not influenced by the HRE concentration in the core region when the thickness of the HRE-rich shell was more than about 15 nm, but only the H_A of the HRE-rich shell determined the coercivity of the diffused magnets.[18]

Magnetic domain observation is helpful for understanding the magnetization reversal mechanism of sintered Nd–Fe–B magnets. The observation of domains with applied magnetic fields at elevated temperature indicated a decrease in the coercivity of sintered Nd–Fe–B magnets at high temperature, attributed to the reduction of H_A.[19] There has been much re-

[†]Corresponding author. E-mail: caoxuejing@nimte.ac.cn

© 2023 Chinese Physical Society and IOP Publishing Ltd

search on Tb diffusion in different forms, such as inorganic Tb compounds, Tb metals and Tb-containing alloys.[10,20–25] However, under an applied magnetic field, how magnetization reversal and its propagation process occur and the impact of Tb diffusion on the magnetization reversal process have not yet been sufficiently discussed. Therefore, it would be worthwhile to intensively research the demagnetization mechanism of annealed and TbF_3-diffused sintered Nd–Fe–B magnets in order to fully understand the coercivity mechanism and maximize the coercivity. In this paper, using a magneto-optical Kerr microscope and the step method, we systematically investigate the influence of Tb diffusion on the dynamic domain evolution and demagnetization behavior of sintered Nd–Fe–B magnets, further illuminating the correlation between microstructure and magnetic properties and leading to a full understanding of the mechanism of coercivity enhancement.

2. Experimental details

Sintered Nd–Fe–B magnets without added HRE elements of composition (Pr, $Nd)_{30}M_{1.25}Fe_{bal}B_1$ (M = Al, Cu or Co, wt.%) were prepared using the powder metallurgical method. The as-sintered magnets without any post-sintering heat treatment were cut into small pieces with a thickness of 3 mm. The magnets as the anode and steel plates as the cathode were both immersed in an ethanol-based TbF_3 suspension. Electrophoretic deposition (EPD) was carried out at a DC voltage of 30 V–100 V for different times to control the thickness of the TbF_3 coating. After the EPD process, even TbF_3 coatings covered the whole surface of the as-sintered magnets. For comparison, the TbF_3-coated magnets and the as-sintered magnets were all treated at 900 °C for 10 h and subsequently annealed at 490 °C for 2 h in a vacuum; these are called the TbF_3-diffused samples and the annealed samples, respectively.

The magnetic properties were measured by a NIM-500C magnetic measuring device and the minor loops under various applied fields were obtained using a physical properties measurement system (PPMS-9, Quantum Design). Backscattered electron images and elemental distributions were acquired using a scanning electron microscope (SEM) (Quanta FEG 250) equipped with an energy dispersive x-ray spectrometer (EDS) (Oxford INCA system). Magnetic domain observations in exactly the same area were done using a magneto-optic Kerr microscope (Evico Magnetics GmbH). The range of the applied magnetic field in the horizontal direction was from 1300 mT to −1300 mT.

3. Results and discussion

Figure 1 shows the demagnetization curves of the annealed sample and the TbF_3-diffused sample at room temperature. It is clear that the coercivity of the annealed magnet is 15.3 kOe, while the TbF_3-diffused magnet shows a much higher coercivity of 25.2 kOe. Compared with the annealed sample, the increase in coercivity is 9.9 kOe and the reduction in the remanence after TbF_3 diffusion is about 0.8 kGs. During diffusion, Tb atoms substituted for Nd in the matrix grains, resulting in a reduction in the remanence due to antiferromagnetic coupling between Fe and Tb. The remanence was measured when the surface layer had not been removed. The squareness value of the TbF_3-diffused sample decreased due to the inhomogeneous distribution of Tb element. The demagnetization curves indicate that the coercivity can be enhanced efficiently using TbF_3 diffusion by the EPD method.

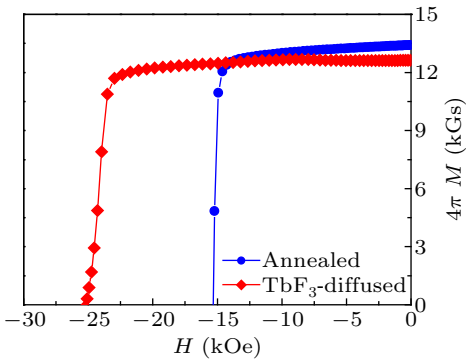
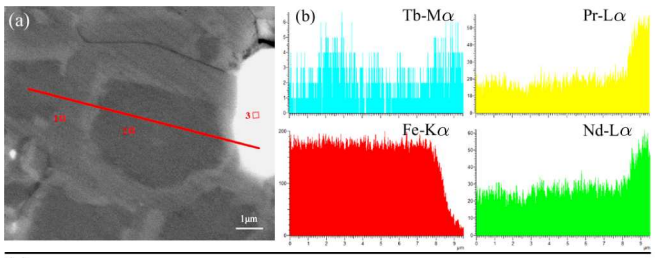


Fig. 1. Demagnetization curves of the annealed sample and the TbF_3-diffused sample.

Figure 2 shows cross-sectional SEM images and the EDS concentration line profiles of Pr, Nd, Tb and Fe across the matrix grain of the TbF_3-diffused magnet. We can see that the Tb-rich core–shell structure, which was clearly visible in the back-scattered image as a gray reaction phase surrounding the dark $Nd_2Fe_{14}B$ grains, is well developed after TbF_3 diffusion. The thickness of the Tb-rich shell near the surface is about 1.9 μm, as shown in Fig. 2(a). Because of the Tb element gradient diffusion, the size of the Tb-rich core–shell structure inside the magnet is dependent on the distance from the surface. The thickness of the Tb-rich shell gradually becomes thinner with increasing depth. The Tb-rich core-shell distribution in the TbF_3-diffused magnet was maintained to a depth greater than 500 μm.

From the Tb concentration line profile across the whole grain, we find that there are strong Tb Mα peaks in the outer region of the matrix grain (Fig. 2(b)). This indicates that Tb diffused into the magnet and formed a Tb-rich $(Nd, Tb)_2Fe_{14}B$ core–shell phase. To detect the distribution of Tb in the grains, the EDS results from the outer region to the core region of the matrix grain are shown in Fig. 2(c). The Tb concentration presents a gradient distribution, and gradually decreases from the shell to the core areas of the grain, ranging from 4.73 wt% to 0.08 wt%. That is to say, Tb element hardly entered the center of the main phase and was not uniformly distributed in the grain, which can effectively reduce the amount of HRE elements. The higher H_A of the Tb-rich shell may impede the

nucleation of reverse magnetic domains in the matrix grains, promoting the increase in coercivity.[4,6]



(c)

Position	Element (wt%)							
	Pr	Nd	Tb	Fe	Al	Co	F	O
1	8.00	13.29	4.73	70.32	0.61	0.99	1.03	1.03
2	10.21	15.54	0.08	70.21	0.58	0.92	1.16	1.30
3	27.85	30.63	1.24	15.49	0.37	0.57	18.73	5.12

Fig. 2. (a) Cross-sectional SEM image of the TbF_3-diffused sample. (b) The EDS concentration line profiles of Pr, Nd, Tb and Fe taken from the red line in part (a). (c) The EDS element analysis results for the selected areas in part (a).

To further study the magnetization reversal process in sintered Nd–Fe–B magnets, the domain evolution of the *in situ* Kerr domain images with different applied magnetic fields for the annealed sample and the TbF_3-diffused sample was observed using a magneto-optical Kerr microscope. The *c*-axis of the annealed sample and the TbF_3-diffused sample was both in-plane. During observation, the applied magnetic field was ramped manually from +1300 mT to −1300 mT. Figure 3 shows the SEM image and the *in situ* Kerr domain images of the annealed magnet at different applied fields. As shown in Fig. 3(a), in the annealed magnet, the grain boundary phase is not continuous, and many adjacent hard magnetic grains have direct contact with each other. In the Kerr domain images, the direction of the external magnetic field applied on the sample is antiparallel to the magnetization direction of the magnet. Before observation with the magneto-optical Kerr microscope, the sample was first magnetized with a 5 T applied magnetic field using a pulse magnetizer. After magnetization by a 5 T external field, almost all grains exhibit single-domain state. However, there are still a few grains with multi-domain structure, mainly because of the absence of the grain boundary phase in the polished grains near the surface. During demagnetization, while the applied magnetic field changed to +700 mT nucleation of the first reversed domain was observed, and then the domain state in one grain transformed from the single-domain state to the multi-domain state, as shown in Fig. 3(c). In the magnetization reversal process, these low-coercivity multi-domain grains had a higher potential to act as initiators, where the reversed domains would prefer to form. The reversed domains grew and spread through many adjacent grains when the applied field was further decreased to −150 mT, as indicated by the dashed-line ellipses in Fig. 3(f). Cascade-type domain propagation was observed and the degree of simultaneous magnetization reversal increased as the applied field was lowered. At an applied field of −300 mT, some grains were inversely saturated. All grains were inversely saturated upon subjecting the sample to a field value of −1200 mT (Fig. 3(j)).

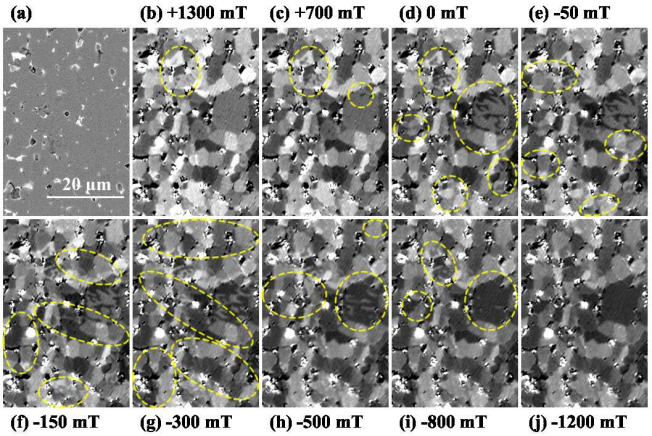


Fig. 3. The annealed sample: (a) cross-sectional SEM image and (b)–(j) *in situ* Kerr domain images at different applied fields.

As shown in Fig. 4(a), in the TbF_3-diffused sample, the Tb-rich $(Nd, Tb)_2Fe_{14}B$ shell structure is well developed in the outer region of the hard magnetic grains. Furthermore, the Nd-rich grain boundary phase is more continuous and thicker than that of the annealed sample. During the substitution of Tb for Nd in the $Nd_2Fe_{14}B$ grain to form the Tb-rich $(Nd, Tb)_2Fe_{14}B$ phase, excess Nd was ejected from the matrix grains and preferred to move to the grain boundaries. As a result, the ejected Nd made the grain boundary phase become more continuous and thicker during the TbF_3 diffusion process. However, in the *in situ* Kerr domain images there is no significant difference between the core and shell areas in a single grain distinguished from the domain contrast because of the low sensitivity of the magneto-optic Kerr microscope.[26] The TbF_3-diffused magnet showed a distinct difference in the magnetization reversal and domain propagation process compared with the annealed magnet. In the remanent state, no formation of reversed domains was observed (Fig. 4(c)). Unlike the case of the annealed magnet, the first magnetization reversal in the TbF_3-diffused magnet appeared at a field of −200 mT, and the magnetic domain state in one grain changed from the single-domain state to the multi-domain state, as marked with dashed-line ellipses in Fig. 4(d). This reversal occurred at a larger field than for the annealed magnet. The reverse grains were weak points, from where the magnetization reversal propagated to their adjacent grains. While the applied field further changed to −450 mT, the reverse magnetic domains gradually spread inside the same grains, and the number of grains with reversed domains increased. The reversed domains continued to expand and spread to the adjacent grains at a larger applied field, i.e., −550 mT (Fig. 4(f)), the field

at which some grains were reversely saturated compared with the annealed sample. At higher applied fields, cascade domain propagation is observed in a few grains (Figs. 4(g) and 4(h)). At the same time, the number of neighboring grains influenced by the simultaneous magnetization reversal in the TbF_3-diffused sample was smaller than in the annealed magnet, indicating that the degree of simultaneous magnetization reversal was reduced for the TbF_3-diffused magnet with high coercivity. Under the maximum applied magnetic field of the magneto-optic Kerr microscope, all grains were saturated inversely (Fig. 4(j)). Compared with Figs. 3(a) and 4(a), the microstructure of the magnets changes obviously after TbF_3 diffusion, therefore, the external field at which the first magnetization reversal and simultaneous magnetization reversal occurred is dependent on the microstructure of the magnets. The Tb-rich (Nd, Tb)$_2$Fe$_{14}$B shell with a much higher magnetocrystalline anisotropy field formed in the outer region of the hard magnetic grain after diffusion prevented the nucleation and propagation of the reversed domain in the $Nd_2Fe_{14}B$ grains. The external magnetic field applied during demagnetization for the TbF_3-diffused sample was much larger than that for the annealed magnet, leading to a higher coercivity.

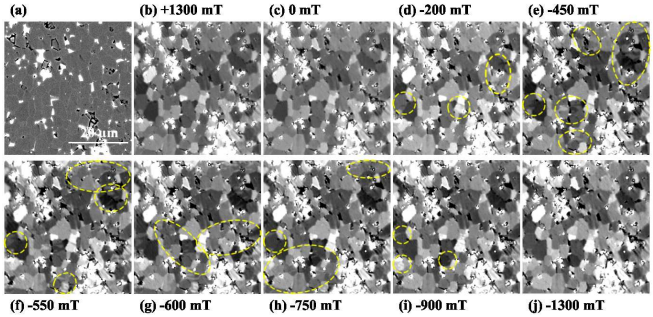


Fig. 4. The TbF_3-diffused sample: (a) cross-sectional SEM image and (b)–(j) *in situ* Kerr domain images at different applied fields.

Figure 5 shows the minor loops during demagnetization of (a) the annealed and (b) the TbF_3-diffused magnets measured by the step method. The samples were first fully magnetized with an applied magnetic field of 5 T before the demagnetization measurements. In the annealed magnet, when the external magnetic field was near 0 T or the field was less than -1.6 T, the minor loops under each applied field show a similar shape. In these loops, the values of the polarization $J(H_{\rm appl})$ and the remanence $J_{\rm r}(H_{\rm appl})$ in the same cycle under the magnetic field ($H_{\rm appl}$) are almost the same. The same polarization indicates that once the magnetization reversal occurred at the applied field $H_{\rm appl}$ it retains the magnetic structure even if the external field drops to zero. However, under an applied field of -1.0 T to -1.6 T, the shape of the loops changes slightly. When the polarization decreased to $J(H_{\rm appl})$ with an applied field $H_{\rm appl}$, the polarization obviously increases to the remanence at $J_{\rm r}(H_{\rm appl})$. The physical explanation for this increase in polarization is that it stemmed from the reproduced domain wall motion (RDWM), $J_{\rm RDWM}$, in accordance with the results of susceptibility measurements.[27] Some regions returned to multi-domain state while the external field was lower than the demagnetizing field. The reproduced multi-domain regions (RMDR) was generated by nucleation of the magnetization reversal center and the continuous propagation of the reversed region to their neighboring area. In contrast, the minor loops of the TbF_3-diffused sample in Fig. 5(b) only had small RDWM, especially under an applied field of -2.2 T to -3.0 T, and the increases in $J_{\rm RDWM}$ were different from those of the annealed sample.

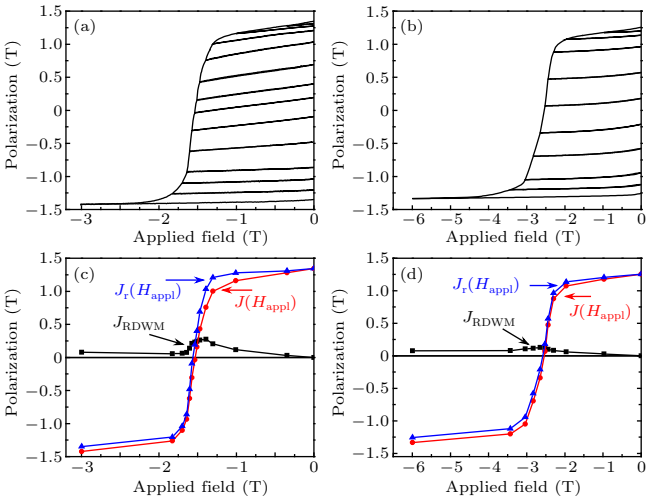


Fig. 5. Results of step method measurements in (a) the annealed sample and (b) the TbF_3-diffused sample, as well as the separated RDWM using the equation $J_{\rm RDWM} = J_{\rm r}(H_{\rm appl}) - J(H_{\rm appl})$ for (c) the annealed sample and (d) the TbF_3-diffused sample.

Figures 5(c) and 5(d) show the $J_{\rm RDWM}$ values calculated from $J_{\rm RDWM} = J_{\rm r}(H_{\rm appl}) - J(H_{\rm appl})$ in the measured loops, shown in Figs. 5(a) and 5(b) for the annealed and TbF_3-diffused magnets. The $J_{\rm RDWM}$ values exactly correspond to the polarization change caused by RDWM as indicated in the minor loops. The results show clearly different behavior in the RDWM between the annealed and TbF_3-diffused magnets. In the annealed sample, $J_{\rm RDWM}$ was very small for applied fields from 0 T to -1.0 T, but increased in applied fields below -1.0 T and showed a large $J_{\rm RDWM}$. The $J_{\rm RDWM}$ gradually decreased when the applied field reduced from -1.4 T to about -1.6 T. In contrast to the annealed sample, $J_{\rm RDWM}$ of the diffused sample was small during demagnetization. The maximum $J_{\rm RDWM}$ decreased with increasing coercivity in the annealed sample ($J_{\rm RDWM} = 0.29$ T) and the TbF_3-diffused sample ($J_{\rm RDWM} = 0.13$ T). The fraction of the maximum $J_{\rm RDWM}$ to the saturation polarization ($J_{\rm s}$), $J_{\rm RDWM}/J_{\rm s}$, was utilized for defining the maximum volume fraction of the regions where the multi-domain structure returned during demagnetization. The sample which had a big RMDR volume ratio presented a relatively large $J_{\rm RDWM}$ and small coercivity. This was because when the value of $J_{\rm RDWM}/J_{\rm s}$ in the sample was large,

the volume ratio of the reproduced multi-domain regions was large; therefore the process of expansion to the surrounding area from the magnetization reversal region was easy. The increased coercivity in the TbF_3-diffused magnet can be mainly attributed to the more difficult nucleation of magnetic reversed portions due to the increased H_A.

4. Conclusion

The magnetic properties, microstructure and domain structure of sintered Nd–Fe–B magnets with and without TbF_3 diffusion by electrophoretic deposition technology were studied. After TbF_3 diffusion, the coercivity was significantly enhanced from 15.3 kOe to 25.2 kOe. The Tb-rich (Nd, $Tb)_2Fe_{14}B$ shell phase in the outer region of the matrix grains was well developed in the TbF_3-diffused sample. The first magnetization reversal and the dynamic successive domain propagation process were found using a magneto-optical Kerr microscope. In the annealed magnet, cascade propagation of the reversed domain throughout many neighboring grains was observed. In contrast, the magnetization reversal appeared at a larger applied field and the degree of simultaneous magnetization reversal decreased in the TbF_3-diffused magnet. By the step method, domain wall motion was observed, and domain wall motion was generated in the RMDR during demagnetization after full magnetization. The maximum J_{RDWM} decreased with increasing coercivity, and varied from $J_{RDWM} = 0.29$ T for the annealed sample to $J_{RDWM} = 0.13$ T for the TbF_3-diffused sample. The increased coercivity in the diffused sample is mainly attributed to the more difficult nucleation of the magnetic reversed region owing to the enhancement of the magneto-crystalline anisotropy field by Tb diffusion.

Acknowledgments

Project supported by the National Natural Science Foundation of China (Grant No. 52101238), the “Pioneer” and “Leading Goose” Research and Development Program of Zhejiang (Grant No. 2021C01190), and Major Project of Ningbo Science and Technology Innovation 2025 (Grant No. 2020Z046).

References

[1] Sagawa M, Fujimura S, Togawa N, Yamamoto H and Matsuura Y 1984 *J. Appl. Phys.* **55** 2083
[2] Gutfleisch O, Willard M A, Brück E, Chen C H, Sankar S G and Liu J P 2011 *Adv. Mater.* **23** 821
[3] Cao X J, Chen L, Guo S, Di J H, Ding G F, Chen R J, Yan A R and Chen K Z 2018 *AIP Adv.* **8** 056222
[4] Hirosawa S, Matsuura Y, Yamamoto H, Fujimura S, Sagawa M and Yamauchi H 1986 *J. Appl. Phys.* **59** 873
[5] Fukagawa T, Hirosawa S, Ohkubo T and Hono K 2009 *J. Appl. Phys.* **105** 07A724
[6] Hrkac G, Woodcock T G, Freeman C, Goncharov A, Dean J, Schrefl T and Gutfleisch O 2010 *Appl. Phys. Lett.* **97** 232511
[7] Löewe K, Brombacher C, Katter M and Gutfleisch O 2015 *Acta Mater.* **83** 248
[8] Ma T Y, Wang X J, Liu X L, Wu C and Yan M 2015 *J. Phys. D: Appl. Phys.* **48** 215001
[9] Xu F, Wang J, Dong X, Zhang L and Wu J 2011 *J. Alloys Compd.* **509** 7909
[10] Nakamura H, Hirota K, Shimao M, Minowa T and Honshima M 2005 *IEEE Trans. Magn.* **41** 3844
[11] Soderžnik M, Rožman K Ž, Kobe S and McGuiness P 2012 *Intermetallics* **23** 158
[12] Cao X J, Chen L, Guo S, Chen R J, Yan G L and Yan A R 2016 *Scr. Mater.* **116** 40
[13] Cao X J, Chen L, Guo S, Li X B, Yi P P, Yan A R and Yan G L 2015 *J. Alloys Compd.* **631** 315
[14] Li D S, Suzuki S, Kawasaki T and Machida K 2008 *Jpn. J. Appl. Phys.* **47** 7876
[15] Ji W X, Liu W Q, Yue M, Zhang D T and Zhang J X 2015 *Physica B* **476** 147
[16] Sepehri-Amin H, Ohkubo T and Hono K 2013 *Acta Mater.* **61** 1982
[17] Cao X J, Chen L, Guo S, Fan F C, Chen R J and Yan A R 2017 *Scr. Mater.* **131** 24
[18] Oikawa T, Yokota H, Ohkubo T and Hono K 2016 *AIP Adv.* **6** 056006
[19] Takezawa M, Ogimoto H, Kimura Y and Morimoto Y 2014 *J. Appl. Phys.* **115** 17A733
[20] Liu W Q, Chang C, Yue M, Yang J S, Zhang D T, Zhang J X and Liu Y Q 2014 *Rare Met.* **36** 718
[21] Watanabe N, Itakura M, Kuwano N, Li D S, Suzuki S and Machida K I 2007 *Mater. Trans.* **48** 915
[22] Lu K C, Bao X Q, Tang M H, Chen G X, Mu X, Li J H and Gao X X 2017 *Scr. Mater.* **138** 83
[23] Jin L, Ding G F, Zhu J H, Jin Z H, Zheng B, Guo S, Chen R J, Yan A R and Liu X C 2021 *J. Alloys Compd.* **870** 159375
[24] Chen G X, Bao X Q, Lu K C, Lv X K, Ding Y, Zhang M, Wang C, Gao X X 2019 *J. Magn. Magn. Mater.* **477** 17
[25] Zhao L Z, He J Y, Li W, Liu X L, Zhang J, Wen L, Zhang Z H, Hu J W, Zhang J S, Liao X F, Xu K, Fan W B, Song W Y, Yu H Y, Zhong X C, Liu Z W and Zhang X F 2021 *Adv. Funct. Mater.* **32** 2109529
[26] Helbig T, Loewe K, Sawatzki S, Yi M, Xu B X and Gutfleisch O 2017 *Acta Mater.* **127** 498
[27] Kobayashi K, Nimura Y, Urushibata K and Hayakawa K 2018 *J. Magn. Magn. Mater.* **451** 493